Absorption of High-Intensity Subpicosecond Lasers on Solid Density Targets

J. Denavit

University of California, Lawrence Livermore National Laboratory, P.O. Box 808, Livermore, California 94550

(Received 19 June 1992)

The absorption of subpicosecond (≈ 100 fs) high-intensity ($I \approx 10^{20}$–10^{21} W/cm^2) laser pulses normally incident on solid density targets is examined by particle simulations, which include electron scattering. For targets which are overdense by factors exceeding 100, electrons accelerated by the ponderomotive force of the laser couple their energy electrostatically to the ions and the absorption efficiency into the ions scales as $I^{1/2}$. For example, absorption in a carbon target is only a few percent, but a large fraction of the absorbed energy is transferred to the ions.

PACS numbers: 52.25.Rv, 52.40.Nk, 52.65.+z

Recent technology has made possible the generation of subpicosecond laser pulses, which can be focused to very high intensities $\approx 10^{18}$ W/cm^2 [1,2], and further developments are aimed at intensities exceeding 10^{20} W/cm^2. Applications envisioned for these lasers, such as the generation of short x-ray pulses [3], require absorption of the laser light in solid-density plasmas which exceed the critical density by factors $\approx 10^2$ to 10^3. At intensities below 10^{18} W/cm^2 absorption occurs by collisional electron heating [4]. However, at higher intensities, the electrons acquire high energies for which this collisional absorption mechanism becomes ineffective. In the high-intensity regime ($I > 10^{18}$ W/cm^2), absorption involves nonlinear kinetic effects which can best be studied by particle simulation methods. Such simulations have been done by Wilks *et al.* [5] for absorption in relatively low-density plasmas, approximately 4 times overdense. In this case the absorbed laser energy is deposited primarily in electrons, which are accelerated to the MeV range.

This Letter presents particle simulations of absorption in solid density plasmas which are 10^2 to 10^3 overdense and reports the first results in this new regime. The most important result is the coupling of a large fraction of the absorbed energy to *energetic ions*. For 0.8-μm light at an intensity of 10^{20} W/cm^2 normally incident on a carbon absorber, ions acquire a velocity $\approx 10^8$ cm/s and are compressed to 2 or 3 times solid density. The bulk of the electrons remains at energies ≈ 20 keV and half of the absorbed energy goes to ions. The absorption efficiency in this case is only $\approx 1\%$ but increases with higher intensity. In the high-intensity limit, momentum conservation yields simple relations for the ion velocity, $u_i = 2(I/\rho c)^{1/2}$, and for the absorption efficiency into the ions, $\eta_i = 2(I/\rho c^3)^{1/2}$. Here, I denotes the laser intensity, $\rho = n_i m_i$ is the absorber density, n_i is the ion density, m_i is the ion mass, and c is the speed of light.

These results were obtained from particle simulations done with a one-dimensional electromagnetic and relativistic code based on the EM1 algorithm [6]. This method allows a fully nonlinear kinetic treatment of plasma dynamics for arbitrary densities and intensities provided that the time step is small compared to the electron plasma and cyclotron periods. Electron scattering due to collisions with the ions is included using a Monte Carlo method applied at each time step, in a frame moving at the local drift velocity of the ions [7]. The simulations do not include ionization and are initialized with a preformed cold plasma at solid density.

The basic geometry, Fig. 1, considers normally incident light on a thin foil absorber, which typically consists of fully ionized carbon, 600 Å thick. This gives an electron density $n_e = 6.7\times 10^{23}$ cm^{-3}, a plasma frequency $\omega_p = 4.6 \times 10^{16}$ s^{-1}, and a collisionless skin depth $c/\omega_p = 65$ Å. For the wavelength of 0.8 μm considered in most of the simulations the critical density is $n_c = 1.7\times 10^{21}$ cm^{-3} and the absorber is overdense by a factor $n_e/n_c = 390$. The laser intensity rises in 7 fs and remains constant out to 25 fs, representing approximately a fourth of a typical 100-fs pulse without a prepulse. The skin depth is adequately resolved with a cell size $\Delta x = 2$ Å requiring a time step $\Delta t = \Delta x/c = 0.67\times 10^{-3}$ fs and 37 500 time steps in a simulation. The highest intensity considered in the simulations, $I = 10^{21}$ W/cm^2, gives a maximum magnetic field of 5.7×10^9 G, approximately twice the incident field. The corresponding gyrofrequency is $\omega_c = 10^{17}$ s^{-1}, whence $\omega_c \Delta t \leq 0.067 \ll 1$. For an electron temperature of 20 keV, typically found in the simulations, the thermal velocity is $v_{th} = 6\times 10^9$ cm/s and the Debye length is $\lambda_D = v_{th}/\omega_p = 13$ Å. Most simulations were done with $N_p = 4000$ particles for each species, corresponding to 85 particles per Debye length. A number of computations were also done with $N_p = 16000$ and 64000 or with $\Delta x = 0.5$ Å without significant differences in the results.

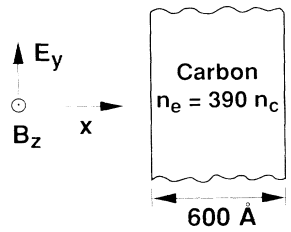

FIG. 1. Geometry of absorbing foil and incident light wave.

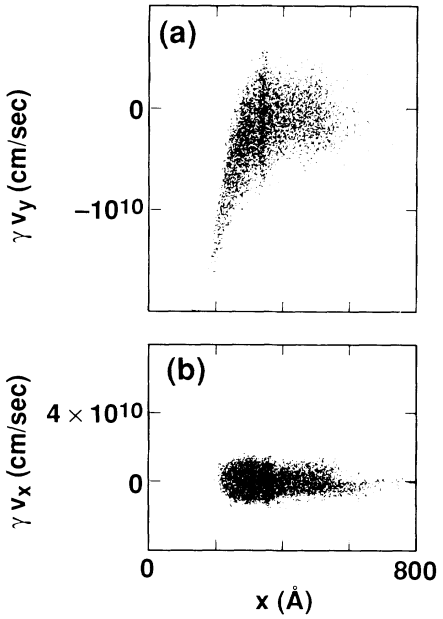

FIG. 2. Electron phase planes γv_y vs x and γv_x vs x at 22 fs from a collisional simulation of a carbon absorber with 0.8-μm light at 10^{20} W/cm^2.

Similar simulations with $Z=4$ show that the results reported here do not depend critically on the ionization level.

The results of a particle simulation at 22 fs, with intensity $I=10^{20}$ W/cm^2 are shown in Figs. 2, 3, and 4. The oscillatory motion of the electrons due to the laser electric field is clearly seen in the transverse electron phase plot, Fig. 2(a). The oscillatory velocity extends ≈ 100 Å into the plasma, as expected from the estimated skin depth, and the mean oscillatory velocity is $\approx 0.3c$. This plot also shows that there is a significant velocity spread due to scattering. The plasma initially occupied a region from $x=0$ to $x=600$ Å and the plots show that the left vacuum interface, which is exposed to the light, has moved approximately 200 Å. For the large magnetic field of the evanescent wave in the plasma and the typical transverse velocities $\approx 0.3c$ seen in Fig. 2(a), the magnetic term of the Lorentz force is as large (or larger) than the electric term. Thus, the electrons are strongly accelerated in the longitudinal (x) direction and acquire large longitudinal velocities as observed in the phase plot of Fig. 2(b).

The ion density profile, Fig. 3, shows that the front of the foil is compressed to 2.4×10^{23} cm^{-3}, more than twice the solid density. There is also a sharp peak at $x=340$ Å, reaching 10^{24} cm^{-3}. Behind this peak, the density falls back to solid density and then falls off as the rear of the foil expands into vacuum. These features are closely related to the ion phase plane shown in Fig. 4. Only a few ions still remain in the region from $x=0$ to $x=200$ Å and at the location of the ion density peak, $x=340$ Å, there is a shock front with partial ion reflection. This

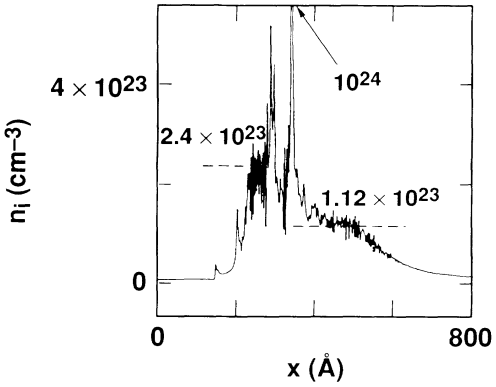

FIG. 3. Ion density profile at 22 fs for the same case as Fig. 2.

shock propagates at a constant velocity, $u_s=1.8\times10^8$ cm/s. Ions to the left of this shock have been accelerated to oscillating velocities averaging 10^8 cm/s. To the right of the shock, the main ion component is stationary, and the reflected ions form a sparse stream which has been accelerated to $\approx 4\times10^8$ cm/s. The ions at the rear of the foil ($x>600$ Å) are also accelerated by expansion into vacuum.

The partial ion reflection and the oscillatory ion velocity displayed in Fig. 4 are characteristic features of a collisionless electrostatic shock [8], which plays an important role in coupling accelerated electrons to the ions. For Mach numbers $M=u_s/c_s<1.6$, where $c_s=(ZT_e/m_i)^{1/2}$ is the ion sound speed, only symmetrical ion-acoustic solitons occur, their maximum potential, $\phi_{\max}$, allowing all the ions to be transmitted. However, at the critical Mach number, $M=1.6$, there is a partial ion reflection, a shock is formed, and the downstream potential (to the left of the shock) becomes oscillatory. This causes the ion velocity to oscillate between u_s at the shock front and a minimum $u_{\min}=(1-\xi)u_s$, where

$$1-0.72\frac{1-R}{1+R}\xi=\exp[-1.28\xi^2]$$

and R denotes the fraction of reflected ions [9]. With $u_s=1.8\times10^8$ cm/s, $M=1.6$ implies an electron tempera-

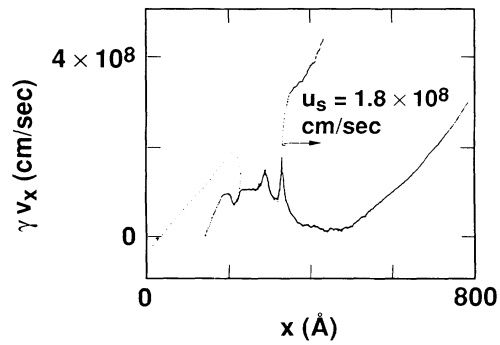

FIG. 4. Ion phase plane at 22 fs for the same case as Fig. 2.

ture $T_e = 26$ keV in the longitudinal (x) direction. This corresponds to a thermal velocity $v_{th} = 6.8 \times 10^9$ cm/s, which is consistent with the phase plot of Fig. 2(b). Assuming a reflection ratio $R = 0.1$, gives $u_{min} = 0.8 \times 10^8$ cm/s and a wavelength $\lambda = 2.5\lambda_D = 45$ Å for the ions velocity oscillations. These values agree approximately with the first oscillation to the left of the shock in Fig. 4. Further oscillations are not clearly seen in Fig. 4, but this may be due to fluctuations in the electron temperature resulting from the oscillating laser field. Note also that this theory does not account for electron scattering or partial reflection of the electrons at the shock front.

The effect of electron scattering was examined by running a collisionless simulation identical to the preceding case. In this collisionless simulation, the longitudinal electron temperature, $T_e \approx 11$ keV, is lower than in the collisional case and most of the ions are reflected by the shock. The large ion reflection ratio is a consequence of the lower temperature, which reduces the shock speed to $u_s = 1.6c_s \approx 1.2 \times 10^8$ cm/s (compared to 1.8×10^8 cm/s in the collisional case). Reflected ions are accelerated at the shock to a velocity $u_i = 2u_s$, while transmitted ions are accelerated to $u_i < u_s$. Therefore, a larger reflection ratio maintains the same rate of increase in ion momentum with a smaller shock speed.

For a simulation similar to the case of Figs. 2–4, but at 10^{21} W/cm^2, the ion phase plane shows that a large fraction, $R \approx 1$, of the ions are now reflected, see Fig. 5. Here the foil initially extends from $x = 0$ to $x = 1000$ Å. Since the absorption efficiency is small, the electromagnetic pressure at the absorber surface is approximately $2I/c$, twice the incident momentum flux. Since most ions do not cross the shock, mass conservation requires $u_i = 2u_s$ and matching the electromagnetic pressure with the rate of increase in ion momentum yields $u_i = 2(I/m_i n_i c)^{1/2}$. For the case of Fig. 5, this gives $u_i = 7.7 \times 10^8$ cm/s and $u_s = 3.85 \times 10^8$ cm/s, which agree with the simulation results. The absorption efficiency into the ions can be expressed as $\eta_i = 2(I/\rho c^3)^{1/2}$, where ρ is the density of the absorber. With a carbon absorber at 10^{21} W/cm^2 this gives 2.6% absorption into the ions, close to the 2.7% absorption observed in the simulation. At this intensity, electron scattering does not have a significant effect and a collisionless simulation gives identical results.

TABLE I. Laser absorption in the bulk of the electron distribution, in hot electrons and in the ions for a carbon target.

I (W/cm^2)	Bulk electrons < 128 keV	Hot electrons > 128 keV	Ions
10^{16}	12.5%	0	0
10^{18}	4.6%	0	0
10^{20}	0.45%	0.23%	0.68%
10^{21}	0.22%	1.03%	2.7%

The absorption efficiencies into the electrons and ions after the intensity has reached its constant value are given in Table I. The table includes simulation results at lower intensities of 10^{16} and 10^{18} W/cm^2. The absorption efficiency into the bulk of the electrons (< 128 keV) is due to collisions. As the intensity is increased, T_e increases and this collisional absorption becomes ineffective. This is clearly seen in Table I and is also in agreement with experiments [3,4]. In contrast, absorption by ions, which is related to the electromagnetic pressure, is negligible at the lower intensities and increases with increasing intensity. The table also lists the absorbed fraction going into hot electrons with energies ranging from 128 keV to several MeV. These electrons appear to be accelerated from the low-density layer which is left behind the receding plasma.

Additional simulations were done for a frozen deuterium absorber, which has a much lower density than carbon, giving an overdensity ratio $n_e/n_c = 24$. For example, with $I = 6.2 \times 10^{19}$ W/cm^2, the electrons are now heated to $T_e \approx 0.5$ MeV and there is a large population of energetic electrons, with energies up to 3 MeV. The larger electron temperature found here is due to the lower value of $n_e/n_c = 24$ (compared to 390 for the carbon case). This increases both the skin depth and the magnitude of the electric field penetrating the plasma, thus driving the electrons to higher energies. The ion phase plane for this case, Fig. 6, is very different from that for the carbon case. There are no reflected ions and an ion-acoustic soliton, propagating at $u_s = 6.4 \times 10^8$ cm/s, is generated. This

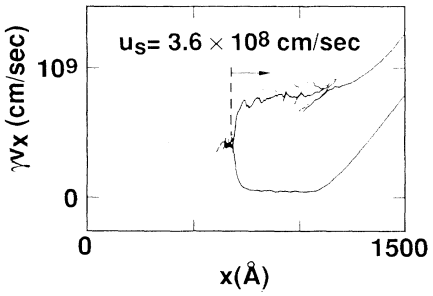

FIG. 5. Ion phase plane at 20 fs for a simulation of a carbon absorber with 0.8-μm light at 10^{21} W/cm^2.

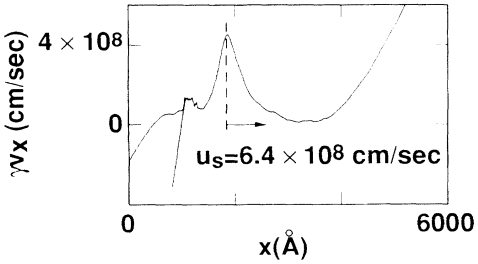

FIG. 6. Ion phase plane at 36.6 fs for a simulation of a frozen deuterium absorber with 0.8-μm light at 6.22×10^{19} W/cm^2.

is a consequence of the larger electron temperature, which raises the ion sound speed. The Mach number is now $M=u_s/c_s=1.3$, less than the critical value of 1.6 corresponding to ion reflection [8]. Similar results were obtained for a carbon absorber at a wavelength of 0.35 μm for which $n_e/n_c=75$.

The present simulations apply only to normal incidence. In the case of P-polarized oblique incidence, the electric field at the plasma interface has a normal component, E_x, and for small absorption efficiencies, $E_x \approx 2E_0\sin\theta$, where θ denotes the angle of incidence. At lower intensities, $I \leq 10^{16}$ W/cm^2, this field component causes a form of resonance absorption by oscillating electrons in the direction perpendicular to the plasma interface [10]. However, at the intensities considered here, the electrons oscillate in the direction perpendicular to the interface even in the case of normal incidence, due to the magnetic term of the Lorentz force, v_yB_z/c, where $B_z \approx 2E_0$. Thus, oblique incidence is expected to become significant for $E_x > v_yB_z/c$, or $\sin\theta > v_y/c$. At an intensity of 10^{20} W/cm^2, Fig. 2(a) shows $v_y/c \approx 0.3$ and the normal incidence results should remain valid for $\theta \ll 17°$. This is confirmed by oblique incidence simulations at $\theta=5°$, 10°, and 30° done by going to a reference frame moving in the y direction with velocity $v_0=c\sin\theta$, for which oblique incidence reduces to a normal incidence [11]. At 5° and 10° incidence, the results are very close to the normal incidence case, while at 30° incidence, more hot electrons are generated and no ion reflection occurs.

The results presented in this Letter show that at high intensities, between 10^{20} and 10^{21} W/cm^2, and for overdensity ratios $n_e/n_c > 100$, laser absorption yields ion acceleration. At these intensities, the radiation pressure of the laser is sufficiently large to accelerate ions to energies in the 100-keV range. Hot electrons with energies ranging up to several MeV are also generated in the thin low-density plasma which forms in front of the solid density interface. This effect is enhanced at large angles of incidence and would also be enhanced by the existence of a prepulse.

For foils a few microns thick, and for typical pulses of 100 fs, the plasma motion during the pulse would be limited to an absorbing layer ≈ 0.1 μm thick, extending over a spot ≈ 10 μm in diameter corresponding to the laser best focus. After termination of the pulse, the resulting ion beam will heat the underlying material by energy deposition. For example, a carbon absorber irradiated at 10^{20} W/cm^2 would produce 60-keV carbon ions. These ions have a velocity of 10^8 cm/s and a slow-down time of 1 ps, and therefore deposit their energy over ≈ 1 μm thickness. The temperatures that can be achieved depend on electron conduction and radiation, and could be computed from fluid codes using the sources of energetic ions and electrons specified by the present simulations.

The author would like to thank his colleagues D. S. Bailey, W. L. Kruer, A. B. Langdon, P. W. Rambo, P. C. Wheeler, and S. C. Wilks for many interesting ideas which have contributed to these simulations. This work was performed under the auspices of the U.S. Department of Energy by Lawrence Livermore National Laboratory under Contract No. W-7405-Eng-48.

[1] P. Main and G. Mourou, Opt. Lett. **13**, 467 (1988).

[2] F. G. Patterson, R. Gonzales, and M. D. Perry, Opt. Lett. **16**, 1107 (1991); see also W. E. White, J. R. Hunter, L. Van Woerkom, T. R. Ditmire, and M. D. Perry, Report No. UCRL-JC-110076, 1992 (to be published).

[3] M. M. Murnane, H. C. Kapteyn, and R. W. Falcone, Phys. Rev. Lett. **62**, 155 (1989).

[4] H. M. Milchberg and R. R. Freeman, J. Opt. Soc. Am. B **6**, 1351 (1989).

[5] S. C. Wilks, W. L. Kruer, M. Tabak, and A. B. Langdon, Phys. Rev. Lett. **69**, 1383 (1992).

[6] C. K. Birdsall and A. B. Langdon, *Plasma Physics via Computer Simulation* (McGraw-Hill, New York, 1976), p. 133.

[7] M. N. Rosenbluth, W. M. MacDonald, and D. L. Judd, Phys. Rev. **107**, 1 (1957).

[8] S. S. Moiseev and R. Z. Sagdeev, J. Nucl. Energy, Part C **5**, 43 (1963); see also D. A. Tidman and N. A. Krall, *Shock Waves in Collisionless Plasmas* (Wiley-Interscience, New York, 1971), pp. 99–112.

[9] The minimum velocity and the wavelength of the oscillations were computed by evaluating the function $F(\phi)$ of Ref. [8] for a flattop ion energy distribution of width $\ll T_e$.

[10] F. Brunel, Phys. Rev. Lett. **59**, 52 (1987); see also Phys. Fluids **31**, 2714 (1988).

[11] P. Gibbon and A. R. Bell, Phys. Rev. Lett. **68**, 1535 (1992).

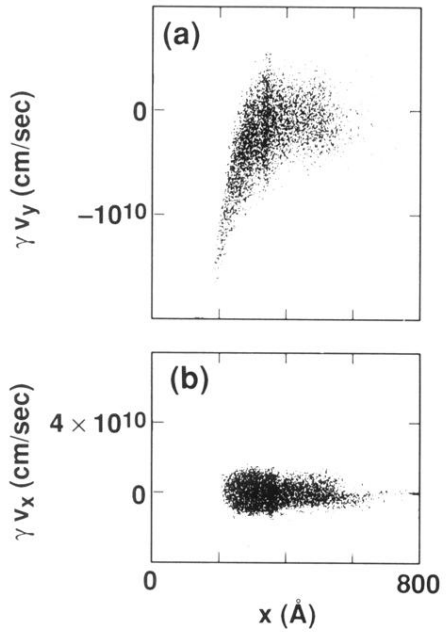

FIG. 2. Electron phase planes γv_y vs x and γv_x vs x at 22 fs from a collisional simulation of a carbon absorber with 0.8-μm light at 10^{20} W/cm^2.